Multi-scale Modeling and Experimental Investigation of Oxidation Behavior in Platinum Nanoparticles

Tom Demeyere,[†] Husn U. Islam,[‡] Tom Ellaby,[‡] Misbah Sarwar,[‡] David Thompsett,[‡] and Chris-Kriton Skylaris[*,†]

[†]*School of Chemistry, University of Southampton, Highfield, Southampton SO17 1BJ, United Kingdom*

[‡]*Johnson Matthey Technology Centre, Blount's Ct, Sonning Common, Reading, United Kingdom*

E-mail: C.Skylaris@soton.ac.uk

Abstract

Understanding the oxidation behavior of Pt nanoparticles (NPs) is crucial for developing durable and efficient catalysts. In this study, we investigate the oxidation of a realistic Pt NP, retrieved from scanning transmission electron microscopy (STEM) images. We use a multistep approach combining ReaxFF and MACE-MP-0 forcefields with Density Functional Theory (DFT) calculations. Our Monte Carlo simulations reveal high oxidation of the nanoparticle, with oxygen penetrating deep into the core. We explore the plausibility of these configurations by carrying out XRD, TEM and EXAFS measurements on samples of various average particle sizes. Progressing in our workflow, we find that 100 ns of thermostated dynamics at 350 K using the ReaxFF forcefield leads to the formation of detached Pt_6O_8 species. To explore the validity of this small platinum-oxide cluster, we first optimize the geometries using the recent MACE-MP-0 forcefield resulting in structures without the species. We then compare both forcefields to DFT calculations showing closer agreement for MACE-MP-0 compared to ReaxFF. Finally, we discuss the electronic structure of our oxidized nanoparticles spanning a whole range of oxygen coverages, finding substantial changes in the Pt-5d and O-2p projected density of states of the platinum structure as the coverage increases. Our findings emphasize the importance of accurately describing the potential energy surface and explicitly modeling oxygen coverage to predict catalytically relevant properties at high potentials. This study aims to provide a foundation for understanding the complex interplay between nanoparticle structure, oxidation state, and catalytic performance, aiming to guide the rational design of advanced catalytic materials.

Introduction

Platinum nanoparticles (Pt NPs) have emerged as important catalysts in various industrial applications, including fuel cells, catalytic converters, and chemical synthesis. However, the long-term performance of Pt NPs can be compromised when exposed to reactive conditions such as the acidic environment in proton-exchange membrane hydrogen fuel cells, potentially

leading to a loss of catalytic activity.[1–4] Oxide species (O^*, OH^*) are present at high potentials due to electrochemical oxidation reactions occurring close to 0.8 V.[5,6] These species are thought to be important site-blockers for the ORR, and oxidized catalysts generally show hindered activity, mainly due to site blocking and altered kinetics.[7] For the ORR oxide saturation is also known to lead to hydrolysis i.e. parasitic, non-electrochemical reactions which might contribute to the high onset potential on platinum-based catalysts.[8] This decline in performance presents challenges for the development of durable and efficient catalysts, emphasizing the need for a better understanding of the complex relationship between reactivity conditions and catalyst performance.[9,10]

Experimental studies on the oxidation of platinum nanoparticles have faced challenges, especially when trying to directly link the oxidation state to the resulting chemical reactivity. Early studies, primarily focused on low-index platinum surfaces in ultra-high vacuum (UHV) conditions[11,12] agreed that atomic oxygen binds on Pt(111) forming a (2x2)-O structure at low temperature,[13–15] with some persistence at higher temperature.[16] These studies also indicated that molecular oxygen is unlikely to be present on Pt(111) at room temperature.[12,16] Platinum catalysts can undergo oxidation even at low pressures, inducing modification of electronic properties and structural changes, such as surface buckling.[17] Recent in-situ studies have advanced our understanding by investigating platinum oxidation under near-ambient pressure conditions for longer exposure times. Fantauzzi et al.[18] reported the oxidation of Pt(111) up to 3 monolayers (ML) through a combination of experimental and theoretical approaches. Furthermore, a study on stepped platinum surfaces revealed the formation of platinum-oxide nanoclusters at a pressure of 1 Torr.[19] Finally, an in-situ study by Ellinger et al.[20] at a partial pressure of 500 mbar and high temperature showed the growth of two atomic layers of bulk-like platinum oxide.

Modern platinum catalysts often consist of deposited platinum nanoparticles, which possibly exhibit complex structures that differ from their perfect counterparts.[21] These structural differences can significantly influence the oxidation behavior and catalytic properties.[22] The

oxidation of these platinum nanoparticles has been extensively studied in the literature, with the formation of platinum-oxide phases reported in numerous studies.[23–29] Saveleva et al.[25] reported the growth of mixed PtO and PtO_2 layers when studying the electro-oxidation of Pt nanoparticles under applied voltage, at 450 K. Additionally Imai et al.[26] characterized the initial platinum-oxide phase to have an α-PtO_2 local structure which transitioned to a β-PtO_2 structure as the oxidation time increased under sustained potential. The presence of an ordered oxide phase was confirmed by other studies under various experimental conditions, with a high dependence on the average particle size, where smaller particles were found to be more prone to oxidation.[27–29]

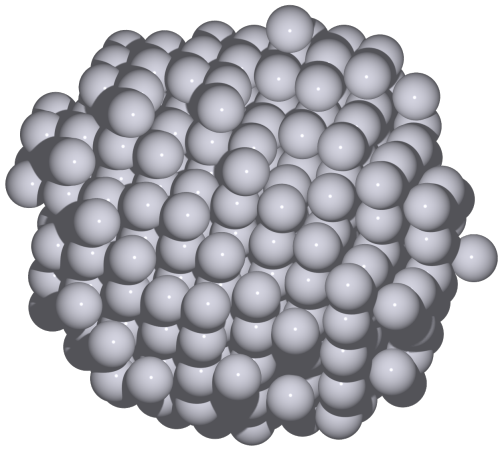

Figure 1: Experimentally reconstructed platinum nanoparticle used in this study. The nanoparticle consists of 353 atoms and was obtained from STEM images.

These studies have provided valuable insights into the oxidation behavior of platinum nanoparticles, but using experimental techniques the underlying mechanisms and implications for catalytic activity are often out of reach. As a result, computational studies have emerged as a valuable tool to complement experimental approaches, providing insights into the oxidation process and helping to overcome the limitations of traditional techniques. Many theoretical studies have supported the claims made by experimental investigations, elucidating the electronic and structural changes induced by oxygen adsorption on platinum catalysts.[30–32] However, the computational modeling of realistic nanoparticles remains largely unexplored,

with most studies focusing on idealized surfaces or perfect nanoparticles,[33,34] leaving room for further computational investigation into the complexity of these systems. Here, we investigate the oxidation behavior of an experimentally reconstructed platinum nanoparticle shown in Figure 1 which was obtained from Scanning Transmission Electron Microscopy (STEM) experimental work.[35] These experimentally reconstructed nanoparticles have been shown to exhibit unique structural features not present in perfect nanoparticles.[36]

We use a multistep approach that combines Monte Carlo simulations with Molecular Dynamics using a fast ReaxFF[37] forcefield, to provide sufficient sampling. We then validate our results by comparing the coordination numbers and bond lengths with experimental data obtained from X-Ray Diffraction (XRD), Transmission Electron Microscopy (TEM) and Extended X-ray Absorption Fine Structure (EXAFS) measurements. We further discuss results obtained with the ReaxFF forcefield by progressively climbing the accuracy ladder, e.g. using the recent MACE-MP-0 model[38] and linear scaling DFT calculations. Finally, we present our results which will aim to highlight multiple key aspects such as the electronic structure modifications of the nanoparticle under oxidation conditions and the difference in thermodynamic and geometric predictions between both forcefields.

Computational Methods

Our workflow is conducted on a platinum nanoparticle composed of 353 atoms which was obtained through a three-dimensional reconstruction process using STEM images from a study of Aarons et al.[35] Our workflow is divided into 5 steps as shown in Figure 2 and will be detailed below.

1. We perform hybrid Monte Carlo-Molecular Dynamics (MC-MD) simulations in the grand canonical ensemble using the LAMMPS software.[39,40] We use a Pt/O/H/C/Ni ReaxFF forcefield developed by Gai et al.,[41] which is originally based on a forcefield from Fantauzzi et al.[42]

This forcefield has been previously used in studies focusing on the oxidation of platinum nanoparticles using various Monte Carlo minimization algorithms.[41] In this study we deviate from these approaches by incorporating dynamics for the platinum atoms. Grand-canonical moves are then performed while the platinum nanoparticle is allowed to move, sampling the canonical ensemble. The main parameter of these simulations is the oxygen chemical potential of the gas reservoir which is calculated assuming ideal gas in Equation 1.

$$\mu_{\mathrm{O}} = \frac{1}{2}[G^{\circ}_{350\mathrm{K}} + k_B T \ln\left(\frac{P}{P^{\circ}}\right) - |E_{\mathrm{DFT}}|] \tag{1}$$

$G^{\circ}_{350\mathrm{K}}$ is the standard Gibbs free energy calculated from $H^{\circ}_{350\mathrm{K}}$ and $S^{\circ}_{350\mathrm{K}}$, the standard enthalpy and entropy respectively, both taken from the NIST-JANAF thermodynamics tables.[43] P is the pressure, P° is the reference pressure and E_{DFT} is the total DFT energy of an oxygen molecule. Throughout the study, we use the pressure as a reference, since it is the only variable term in Equation 1. We study a broad range of pressures from 10^{-25} to 1.0 atm at the same temperature of 350 K.

2. After our MC-MD simulations, we randomly extract 32 geometries throughout the highest pressure run at evenly spaced oxygen coverages, which we can then study systematically.

3. The geometries are then subjected to an additional 100 ns of NVT simulations at 350K. This is done to amplify potential geometrical features such as small platinum-oxide clusters that were previously observed in past studies using similar forcefields. The grand canonical Monte Carlo moves are stopped, and the system is allowed to relax in the canonical ensemble.

4. The geometries are then optimized with both the ReaxFF forcefield and the recent MACE-MP-0 foundation model separately. The MACE-MP-0 model[38] is based on the message-passing version of the Atomic Cluster Expansion (ACE)[44] and is trained on the Material Project database. MACE was recently benchmarked to be one of the most accurate forcefield to predict the energetics of materials across the periodic table.[45]

5. DFT calculations are then performed on the relaxed geometries by both forcefields to

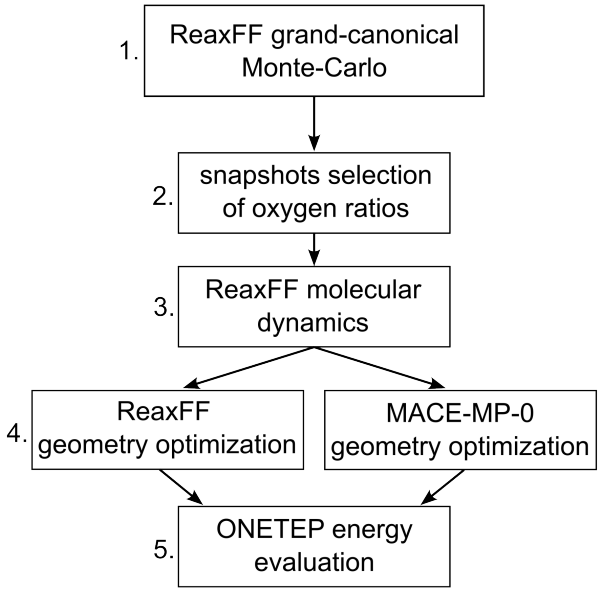

Figure 2: The computational workflow followed in this study. Monte Carlo simulations provide initial configurations, Molecular Dynamics simulations are then performed to relax the geometries and further explore the phase space. Finally, ONETEP linear-scaling DFT calculations are carried out to obtain the electronic structure and refined energetics of the oxidized nanoparticles.

compare them and obtain the electronic structure of the oxidized nanoparticles. Computationally elucidating the electronic structure of such large platinum nanoparticles remains a challenging task, often hindered by the computational expense associated with such calculations. We overcome these limitations by using the ONETEP linear-scaling DFT software,[46] which exhibits a linear scaling behavior with respect to the number of atoms. This enables us to readily access electronic structure calculations for a wide range of nanoparticle sizes and configurations.[47]

Additional computational details for all the methods involved are provided in the supplementary information.

Results

Monte Carlo simulations

Monte Carlo simulations are run until accepted additions and deletions exchange moves stabilize to the same count over the last 5×10^7 exchange moves. This criterion is not applied for higher pressures (1.0, 10^{-2}, and 10^{-5} atm), where the simulations are stopped before reaching this criterion due to low deletion acceptance rate. Throughout the study we will refer to the oxidized nanoparticles using the concept of oxygen ratio N_O/N_{Pt} instead of coverage. This choice is motivated by the difficulty of defining a proper surface area for the nanoparticle and the presence of subsurface oxygen atoms.

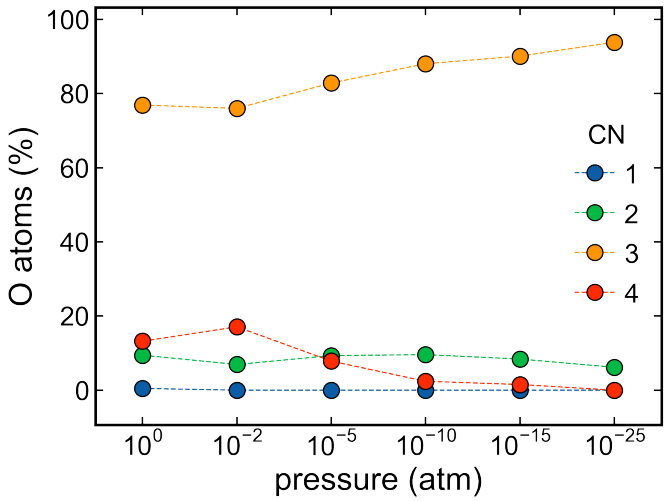

Figure 3: Pressure dependence of oxygen coordination number population. The percentage is calculated with respect to the total number of oxygen atoms for each pressure. Lines are added to guide the eye.

Atomic oxygen tends to adsorb on low-index platinum surfaces on hollow sites (3-fold or 4-fold),[48] this is highlighted in Figure 3 where we report that for most pressures, more than 70% of the oxygen atoms are in a 3-fold coordination. We also report a low number of atomic oxygen binding on bridge sites (2-fold coordination) which does not seem to be impacted by the pressure, indicating that these are specific sites, where oxygen opportunistically binds. After visual inspection, these sites are often found on dangling platinum atoms or on the

edge of the nanoparticle. These sites were previously reported to be the most stable sites for atomic oxygen binding by DFT studies on smaller nanoparticles.[48,49] Finally, as the pressure increases 4-fold subsurface sites become more populated, which occurs between 10^{-10} and 10^{-2} atm when the outer coverage is between 0.7 and 0.9 ML. As suggested by previous DFT studies[50–52] subsurface sites require sufficient lattice disruption to be populated. In our case, sufficient deformation is reached due to oxygen adsorption at the outer shell. We confirmed this hypothesis by performing a full DFT calculation on a smaller nanoparticle with a single oxygen in a subsurface site. We find that the lone oxygen atom moved onto the surface at a 3-fold coordination site during the geometry optimization. Details including pictures of this auxiliary calculation can be found in the supplementary information.

Table 1: Summary of oxygen fractional occupancy N_O/N_{Pt} at different pressures. Our values are reported as oxygen ratio along with an approximation of the outer coverage (calculated as described in the text) in parentheses. Our values are compared to similar studies using similar methods and systems, all reported as coverage, unless specified otherwise.

pressure (atm)	1.0	10^{-2}	10^{-3}	10^{-5}	10^{-10}	10^{-15}	10^{-25}
this work	1.20 (0.90)	1.14 (0.90)	-	0.73 (0.91)	0.47 (0.75)	0.37 (0.59)	0.23 (0.36)
ref$^{\alpha}$	0.8	0.72	-	0.7	0.65	0.5 0.40^{a} 0.36^{b} 0.26^{c}	-
ref$^{\beta}$	-	-	1.38* (1 mbar)	-	-	-	-

$^{\alpha}$Gai et al.[41] Pt(111) (300K), ^{a}octahedral, ^{b}cuboctahedral, ^{c}cubic NPs (500K); $^{\beta}$Kirchhoff et al.[31] 3 nm cuboctahedral NP (400K), *reported as oxygen ratio.

We report the dependence of oxygen ratio versus pressure in Table 1 which further highlights that the strong adsorption energy of atomic oxygen on Pt catalysts leads to sustained coverage even at extremely low pressures. We compare our results to similar studies using similar methods and systems, and also include an approximation of the outer coverage which is done by computing the alpha shape of oxygen atoms and platinum atoms separately.

The coverage is then calculated as the ratio of these two atomic counts. At low pressures, our results compare relatively well with the study of Gai et al.[41] which was done at a lower temperature on a Pt(111) surface. Discrepancies between our results and Pt(111) surface widen when considering the experimental study of Getman et al.[53] where a coverage of 0.48 was reported at a pressure of 10^{-4} atm and a temperature of 353K. A restriction on coverage is identified by the authors to be due to kinetic limitations of O_2, which becomes less favorable as the oxygen coverage increases. When switching to NO_2, a kinetically favorable oxidant, the authors found a coverage of 0.75 ML, closer to our results. We note that our results are not completely comparable to clean surface studies since our nanoparticle has a different surface area and different binding sites and should generally display slightly higher coverages due to stronger binding on a nanoparticle of this size.[54]

Finally, our simulations systematically display a lower oxygen ratio than the studies of Kirchhoff et al.[31] at similar pressures and temperatures. We attribute it to our methodology which differs from the Monte Carlo minimization scheme used in these studies. This minimization scheme includes a full geometry relaxation carried before the acceptance criteria, ultimately leading to faster convergence and higher oxygen ratio, but does not correctly sample the canonical ensemble and resembles more a basin-hopping algorithm. Additionally, our current hybrid MC-MD methodology was not driven by the need to reach specific coverages, but to also include the dynamics of the platinum atoms, to potentially discover interesting geometrical features that might be amplified by including the dynamics. Finally, above our highest oxygen ratio addition moves mainly lead to the formation of O_2 due to saturation, which is less relevant for this study.

To understand the structure of the oxidized nanoparticle we plot the oxygen distribution profiles in Figure 4. The plots represent the spherical density or concentration of oxygen atoms as a function of distance from the center of mass. As the pressure increases, the amount of oxygen penetrating inside the nanoparticle increases, first in subsurface sites at 10^{-5} atm, and then in the core region for pressures above 10^{-2} atm. This is in agreement

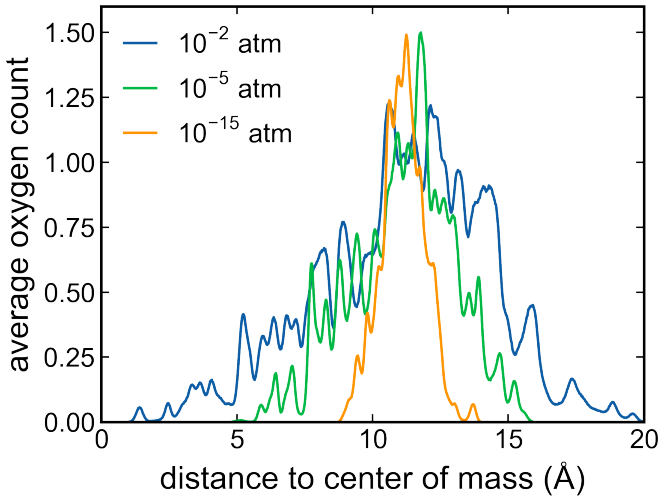

Figure 4: Distribution of oxygen with respect to the center of mass of the oxidized nanoparticle. Subsurface and core oxygen atoms are observed as the pressure increases from 10^{-15} to 10^{-2} atm. No normalization has been applied. The figure have been created by averaging over the 100 ns of NVT simulations in step 3, but is shown here for clarity.

with the previous coordination number analysis shown in Figure 3. Additionally, the same plots reveal a significant amount of lattice strain caused by subsurface and core oxygen atoms at higher pressures. At a pressure of 10^{-15} atm, the outer shell boundary is clearly visible and located approximately 11 Å away from the center of mass. As the pressure increases, the boundary becomes less defined and oxygen atoms are found at distances up to 20 Å away from the center of mass.

Typically, oxidation of metallic nanoparticles is thought to proceed from the surface inwards, with the formation of an oxide shell surrounding a metallic core. The presence of oxygen atoms near the center suggests that under sufficiently oxidizing conditions, platinum nanoparticles can become completely oxidized throughout their entire volume. Various experimental studies have shown that this is most likely not the case for larger nanoparticles (> 2.0 nm).[29,55] For smaller nanoparticles with diameters close or lower than 2.0 nm, previous studies suggest that core oxidation is possible under specific conditions.[27] To further validate these claims and our results, three carbon black-supported Pt catalysts were prepared and characterized by XRD, TEM, and XAS (EXAFS) with the aim of determining average Pt-Pt

and Pt-O distances and coordination numbers as a function of particle size distribution. Measurements were made on prepared catalysts which had been chemically reduced during the synthesis process and subsequently passivated by exposure to air. Our results are summarized in Table 2, the size distributions as measured by TEM gradually increase as a function of Pt loading, XRD measurements showed that the 10 and 20 wt% Pt samples did not show any discrete crystalline Pt domains suggesting that the Pt NPs are both disordered and contain a significant amount of oxide. The 50 wt% Pt sample did show a crystalline Pt domain profile, but the average crystallite size was estimated to be less than 2 nm. The EXAFS CNs support these results with the 10 wt% Pt sample showing Pt-O but no significant Pt-Pt character, the 20 wt% Pt sample showing a mix of Pt-Pt and Pt-O CNs suggesting very small metallic Pt domains which are significantly oxidized. The 50 wt% Pt sample shows significant Pt-Pt character with a relatively small Pt-O component, indicating the presence of metallic Pt NPs with a defined passivated oxide layer at the surface. The Pt-Pt distances for the 20 and 50 wt% Pt samples are 2.76 ± 0.01 Å consistent with that shown by bulk Pt-Pt (2.77 Å), and the Pt-O distances vary between 1.97 and 2.03 Å. Our Monte Carlo simulations are done on a nanoparticle consisting of 353 atoms, whose size is calculated to be 2.03 nm, falling in between the 10 and 20 wt% Pt samples. In Table 2 our simulation done at 1.0 atm shows reasonable agreement with the experimental results, the Pt-Pt coordination number is low, due to the significant oxidation predicted by the Monte Carlo simulations. Similarly, the Pt-O CN is close to the expected range for smaller particle distributions (between 3.4 and 3.6). However, the theoretical Pt-Pt average bond distance is higher than the experimentally measured value, which might be due to higher deformation and lack of a defined oxide phase in the theoretical model. We note that our theoretical coordination numbers were calculated using a distance cutoff determined by the first minima of the corresponding radial distribution function: 3.04 Å for Pt-Pt and 2.3 Å for Pt-O. Due to the particularly high sensitivity of the CNs to the cutoff the comparison with experimental estimate should be taken with caution. The experimental bond distances suggest the presence of Pt(IV) rather than Pt(II) (2.01-2.03

vs. 2.07 Å).[56] Additionally, the mixed oxidation state Pt oxide, Pt_3O_4 shows Pt-O distances of 1.97-2.00 Å.[57,58]

Table 2: Experimental and theoretical coordination numbers and bond distances for Pt-Pt and Pt-O. Theoretical values are averaged over all atoms, which is closer to the experimental definition. The Pt_{353} diameter was estimated by calculating the averaged maximum distance between every two atom pairs of the outer platinum shell.

	cryst. size (nm)	particle size (nm)	coord. number		bond distances (Å)	
			Pt-Pt	Pt-O	Pt-Pt	Pt-O
10 wt%	-	1.7 ± 0.5	-	3.6 ± 0.2	-	2.03 ± 0.01
20 wt%	-	2.4 ± 0.7	2.4 ± 0.7	3.4 ± 0.3	2.76 ± 0.01	2.02 ± 0.01
50 wt%	< 2	2.7 ± 1.3	7.8 ± 0.6	1.9 ± 0.4	2.77 ± 0.01	1.97 ± 0.01
Pt_{353} MC (1.0 atm)	-	2.03	2.68	3.63	2.94	2.05
Pt_{353} MC (10^{-25} atm)	-	2.03	8.57	0.67	2.82	1.97

In contrast with our results, various studies on similar nanoparticle sizes have reported oxidation to occur mainly at the outer platinum shell. Takagi et al.[28] performed *in-situ* Hard X-ray Photoelectron Spectroscopy (HAXPES) measurements at various potentials and reported that for a sample with a size distribution centered around 2.6 nm, only the outer platinum shell was oxidized. The presence of oxygen atoms near the center of the nanoparticle in our simulation is justified by the nature of the Monte Carlo simulations which disregard kinetic aspects. Hence, atomic rearrangement required for oxygen to penetrate deep into the core is bypassed i.e. no activation energy of oxygen diffusion into the platinum lattice, which otherwise, renders this process kinetically unfavorable.[59] Our experimental evidence along with previous experimental work, suggests that the size range between 1.5 nm and 2.5 nm represents a critical transition region where the oxidation behavior changes dramatically.[27] Within this narrow size window, nanoparticles appear to shift abruptly from partial surface oxidation to complete oxidation, indicating a sharp threshold effect. The precise point of this shift likely depends on specific experimental conditions such as temperature, type of oxidant

and partial pressure. Furthermore, the presence of defects or strain in the nanoparticles, which can vary based on synthesis methods may have an influence as well.

Molecular Dynamics

We further progress in our workflow by performing Molecular Dynamics simulations at 350 K for 100 ns. Our interest in extended dynamics can be explained by considering previous literature using similar forcefields where small platinum-oxide clusters have been reported to form.[41] As illustrated in Figure 5, we also report similar dissociation-like events taking place during the dynamics and leading to a number of partially detached Pt_6O_8 species on the nanoparticle. The occurrence of these events strongly depends on the oxygen fraction occupancy, with higher occupancies leading to a greater number of detachments. Each of these events is accompanied by a significant energy reduction as schematically shown in Figure 5a. These species were first reported by Kirchhoff et al.[31,32] where the authors investigated the possibility of a stability region for the small cluster in the aqueous phase with specific charge and spin states.

The resulting geometry after 100 ns of NVT simulations for a high oxygen ratio is shown in Figure 5c where the nanoparticle geometry exhibits significant structural deformations, the morphology appears highly distorted, with pronounced surface irregularities and a loss of the expected quasi-spherical or faceted shape. The structure displays extensive porosity, with the formation of voids and channels permeating throughout the entire nanoparticle. This gives rise to fragmented, loosely bound domains interconnected by these more stable oxidized platinum clusters. The Pt_6O_8 species emerges as a distinctive motif, standing out in contrast to the overall amorphous structure. Importantly, no other such well-defined cluster species can be clearly distinguished within the nanoparticle structure. These structural perturbations collectively contribute to an increased surface-to-volume ratio which should elevate the surface free energy, with the Pt_6O_8 units serving as structural anchors.

If, as described by the forcefield, these events are taking place frequently within 100 ns of

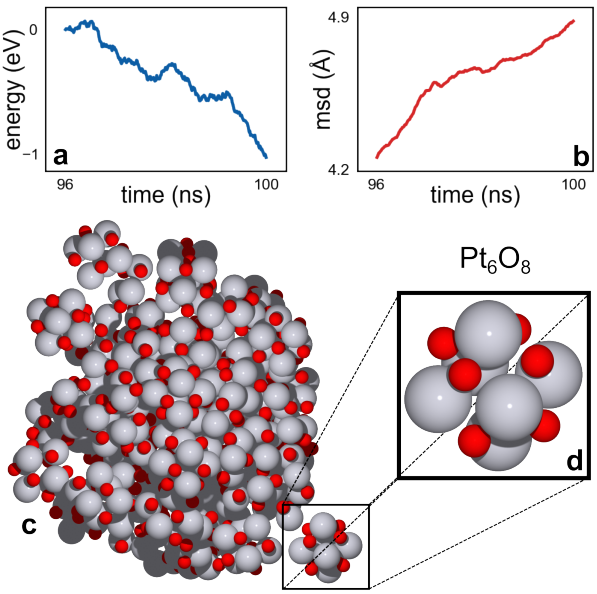

Figure 5: An example of a dissociation event taking place during the dynamics at high oxygen fractional occupancy ($N_O/N_{Pt} > 0.6$). These events lead to an energy reduction (a) and geometrical deformation shown by an increase in mean square deviation (msd) of nuclear coordinates (b). The final state of the nanoparticle after 100 ns is shown with an oxygen ratio of 1.07 (c). A Pt_6O_8 species is partially detached from the nanoparticle (d).

simulation, it would be expected to find experimental evidence of this species even in UHV conditions for pressures above 1 Pa. Despite this, we were not able to find experimental evidence of the existence of the Pt_6O_8 species. Instead, platinum dissolution is believed to occur at the interface at specific potentials, and to be an atomic process that might be influenced by oxide formation, but not via Pt_6O_8 species.[60,61] The presence of this species will be further investigated in the next sections, by performing geometry optimizations with MACE-MP-0 and subsequent DFT calculations.

Geometry optimizations

We select the last snapshots from the previous molecular dynamics run for all our oxygen ratios and perform geometry optimizations. For comparison, we also perform geometry optimizations using the recent MACE-MP-0 model using the same geometries. We quickly notice a global trend where the MACE-MP-0 forcefield attempts to put back the Pt_6O_8

species together with the rest of the nanoparticle, in contrast with the ReaxFF forcefield which keeps the Pt_6O_8 species in a semi-detached state.

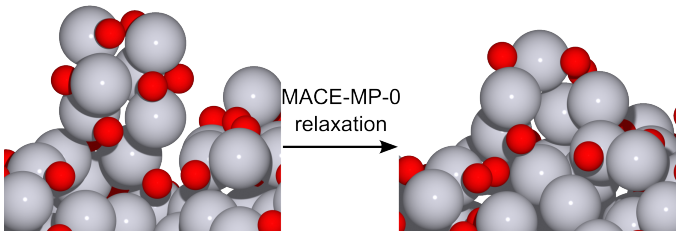

Figure 6: Illustration of the commonly observed phenomena during a MACE-MP-0 geometry optimization, the Pt_6O_8 species is packed back into the nanoparticle.

An example of the process is shown in Figure 6 where the Pt_6O_8 species is packed back together with the rest of the nanoparticle. Although geometry optimizing will only partially change the initial geometry from ReaxFF, these results indicate that MACE-MP-0 would give geometries that do not include Pt_6O_8 species. In order to systematically compare geometries between the two forcefields we define the concept of sphericity score which quantifies the deviation from a perfect spherical shape by calculating the variance in the distances between the centroid and the platinum atoms at the nanoparticle surface.

$$S = \mathrm{Var}[R(\mathcal{S}_{\mathrm{outer}})] \tag{2}$$

$\mathcal{S}_{\mathrm{outer}}$ is the set of atoms belonging to the outer shell, obtained by computing the alpha shape of the nanoparticle, and $R(\mathcal{S}_{\mathrm{outer}})$ represents the distances from each atom in $\mathcal{S}_{\mathrm{outer}}$ to the centroid. The obtained scores are then normalized between 0 and 1 within the dataset, with 0 being the least spherical and 1 being the most spherical nanoparticle. Figure 7 shows the sphericity scores for the entire dataset. Generally, ReaxFF produces geometries with lower sphericity scores, while the geometries optimized using MACE-MP-0 are consistently more spherical. In addition, our sphericity concept is a good measure of the geometrical deformation of the nanoparticle against oxygen ratio. This tendency towards more spherical geometries suggests that MACE-MP-0 favors more compact and densely packed structures, compared to the more irregular structures predicted by ReaxFF.

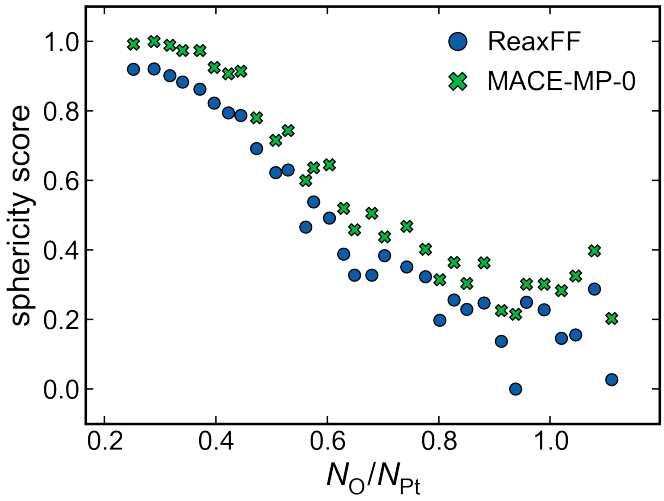

Figure 7: Sphericity scores calculated for geometries predicted by both forcefields against oxygen ratio, the dataset has been scaled between 0 (least spherical) and 1 (most spherical). As the oxygen ratio increases, particles are less spherical. MACE-MP-0 geometry optimizations consistently make the geometries more spherical.

With both of our forcefields having different behaviors in terms of geometrical deformation, we expect that thermodynamic properties will also be different. We further explore these disparities by focusing on thermodynamic aspects, using Equation 3. The equation makes use of the Computational Hydrogen Electrode (CHE) scheme which enables extrapolation of the free energy at different potentials as a posteriori correction.[62] Additionally, this approach also avoids calculations involving atomic or molecular oxygen, which are known to be problematic for DFT.[63]

$$\Delta G_{\mathrm{O}}(U_{\mathrm{SHE}}) \equiv n\Delta\bar{G}_{\mathrm{O}}(U_{\mathrm{SHE}}) = G_{n\mathrm{O}^*} - G_* - nG_{\mathrm{H_2O}} + 2n\left(\frac{1}{2}G_{\mathrm{H_2}} - U_{\mathrm{SHE}}\right) \tag{3}$$

Where $G_{n\mathrm{O}^*}$ is the Gibbs free energy of the nanoparticle with n oxygen atoms, G_* is the Gibbs free energy of the nanoparticle with no oxygen atoms. $G_{\mathrm{H_2O}}$ and $G_{\mathrm{H_2}}$ are the Gibbs free energies of water and dihydrogen in their standard state, respectively. U_{SHE} is the potential of the standard hydrogen electrode. The Gibbs free energies in Equation 3 are often reduced to $G = E_{\mathrm{DFT}} + E_{\mathrm{ZPE}} - TS_{\mathrm{vib}}$ for adsorbates.[64] Considering the large size of our systems we decided to ignore zero-point and thermal contributions for the oxidized

nanoparticles and reduce the Gibbs free energy to the DFT energy, $G \approx E_{\mathrm{DFT}}$. For reference species, the total energy is computed with DFT on the isolated molecule, Zero Point Energies (ZPEs) are available elsewhere[62] (0.27 eV for H_2, 0.56 eV for H_2O), and entropy contributions are taken from the NIST-JANAF thermodynamic tables.[43] In practice Equation 3 is related to the total (ΔG_{O}) or per atom ($\Delta \bar{G}_{\mathrm{O}}$) binding energy of oxygen atoms on the nanoparticle, using water and hydrogen as reference states.

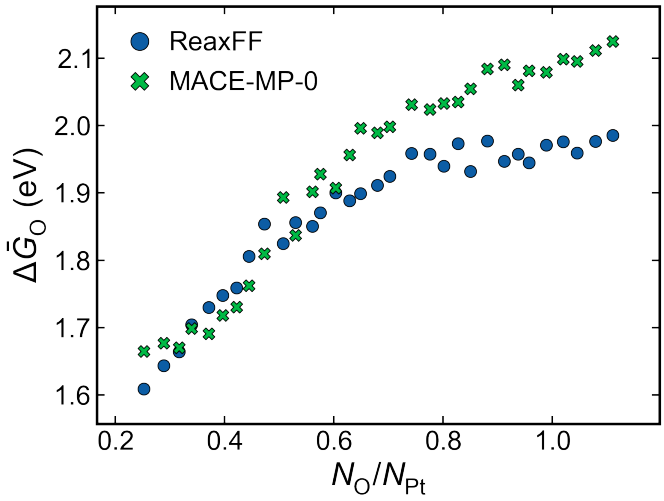

Figure 8: Oxygen binding energy per oxygen atom plotted vs. oxygen ratio calculated using Equation 3. Two regimes can be observed, a linear, monotonic regime for ratios below 0.7, which then plateau at higher ratios. Compared to MACE-MP-0, ReaxFF predicts stronger binding at higher coverages.

We report binding energies per oxygen atom ($\Delta \bar{G}_{\mathrm{O}}$) in Figure 8 for geometry optimized structures using each forcefield. As expected, the binding strength lowers as the coverage increases as the interaction between adsorbates intensifies.[16] From the same figure, two regimes can be distinguished, starting with an initial linear progression for both forcefields. ReaxFF then predicts a near-constant regime for oxygen ratios above 0.7, while MACE-MP-0 is more moderate but still displays a plateauing behavior. This phenomenon was also observed in previous studies of oxidized platinum nanoparticles including experimental evidence.[65] We expect this regime change to be reflected by electronic features, which we will explore in the next section by performing DFT calculations.

Finally, it is possible to calculate the thermodynamic expected oxidation state at a given potential. To do so, we select evenly spaced points in the ΔG_O vs. N_O/N_{Pt} fitting. For each of these points, we calculate the potential dependence using the CHE on a fine grid of U for each oxidized configuration. This process yields a set of linear curves representing the potential dependence for the selected systems. By finding the lowest curve in this set for multiple potential subranges, we determine the thermodynamically favored state at each potential. As a result, we obtain an oxygen ratio vs. potential curve which represents the expected oxidation state across a range of potentials. This process is carried out for both forcefield and shown in Figure 9. Starting at 0.7 V, oxidation steadily grows as the potential increases, which is the expected behavior and in reasonable agreement with previous studies.[66] Our value of onset potential for oxidation is also in reasonable agreement with the one of 0.8 V reported in the literature.[66–69] At high oxygen coverages, we observe a notable difference between the predictions of ReaxFF and MACE-MP-0. When the potential approaches 1.05 V ReaxFF predicts a sharp and almost vertical progression. We link this phenomenon to the experimentally observed place-exchange mechanism, where the oxidation starts to complete, and the nanoparticle evolves towards an oxide phase. This phenomenon was experimentally reported to occur at $\approx$ 1.05 V on platinum nanoparticles and surfaces.[70–73] In our framework the event is transcribed via thermodynamic arguments and is due to the plateauing regime of the Gibbs free energies vs. oxygen ratio. In contrast, MACE-MP-0 predicts a more gradual increase in oxidation, most likely because it does not recognize the oxide phase formed by the ReaxFF forcefield. The potential reported by ReaxFF for the place-exchange mechanism ($\approx$ 1.05 V) is in very good agreement with the reported experimental values. Results before the molecular dynamics (step 3) are also included to highlight the effects that the additional platinum-oxide clusters have on the predicted stability diagram. For ReaxFF we see that the curve is shifted towards lower potentials with the difference between the two curves becoming larger as the potential increases. MACE-MP-0 displays the inverted trend and smaller differences, as the forcefield does not predict the species.

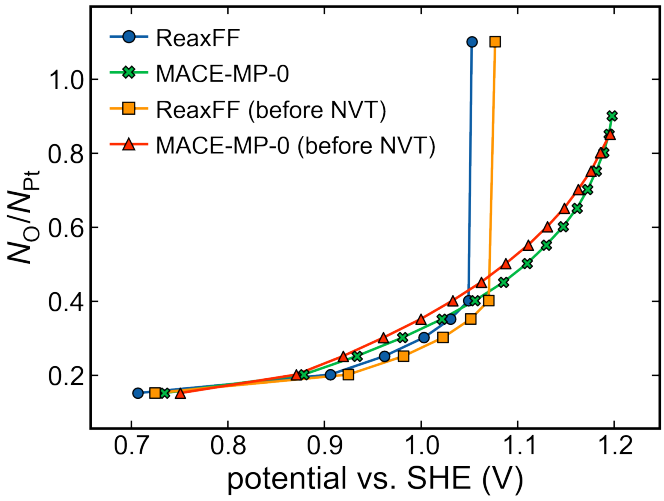

Figure 9: Oxygen ratio vs. potential curves obtained by following the procedure described in the text. Results before the molecular dynamics (step 3) and their MACE-MP-0 geometry optimized version are shown for comparison.

Being able to produce an accurate version of this curve is of paramount importance since oxygen population is suspected to be the cause of the high onset potential of the ORR on Pt for both thermodynamic and kinetic reasons.[69] A catalyst that shifts this curve by 0.1 - 0.2 V would be expected to outperform compared to current catalysts for the ORR. This shift would require the binding energy of the oxygen atoms to be reduced by the same amount across the whole potential range, which was previously done by tuning the nanoparticle size, composition or shape.[4] Performing similar simulations using a universal potential such as MACE-MP-0 would allow for the exploration of these effects, along with external factors such as a support or a solvent, given that these more advanced forcefields retain reasonable accuracy. Additionally, going beyond the CHE approximation will be required to produce an accurate version of Figure 9. For example, our simulations do not account for electrochemical phenomena i.e. electric fields that arise due to the potential drop at the interface. Similarly, in the CHE framework, electrochemical adsorption is represented by a coupled electron-proton transfer,[74] most likely misrepresenting any electrosorption valency phenomena normally involved in these adsorption process.[75]

ONETEP calculations

Finally, we compute electronic properties by performing single-point energy evaluations at the DFT level. Due to the cost of these calculations, we only selected half of our previous dataset of 32 oxygen ratios previously optimized by ReaxFF and MACE-MP-0. This allows for a direct comparison between the two forcefields. Figure 10 reveals that ReaxFF tends to overestimate the binding energy ΔG_{O}, while MACE-MP-0 is in better agreement with DFT. We note that for all our tested oxygen ratios, a geometry optimization with the MACE-MP-0 forcefield also leads to an energy reduction at the DFT level. This reinforces the hypothesis that the Pt_6O_8 species are most probably an artifact due to the parametrization of the ReaxFF forcefield on specific bulk platinum oxides.

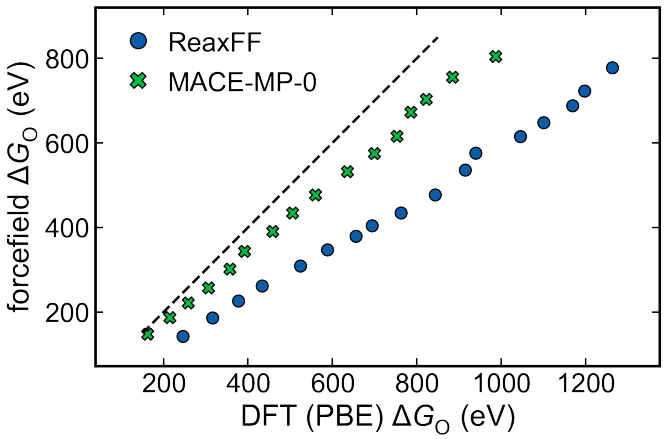

Figure 10: Total binding energies ΔG_{O} predicted by both forcefields plotted against DFT. ReaxFF overestimates the binding strength, while MACE-MP-0 is closer to the DFT results.

In an attempt to explain the saturation regime of oxygen on Pt nanoparticles at high oxygen ratios, we computed the projected density of states (PDOS) of the Pt-5d orbitals (Figure 11a) and the O-2p orbitals (Figure 11b) for a range of oxygen ratios.

As the oxygen ratio increases, the PDOS of the Pt-5d orbital displays a significant peak increase just below the Fermi energy centered around -2.0 eV. In parallel, we observe an important decrease in intensity for states at lower energies as the oxygen ratio increases. As oxygen are added, the Pt-5d PDOS displays a decreased metallic character as the peak

becomes narrower and more localized, indicating a change of the electronic structure towards a platinum-oxide-like cluster. Additionally, the d-band center slightly shifts towards lower energies. In contrast, the O-2p PDOS does not display substantial variations, with only a slight decrease in the peak located at -6.0 eV and the appearance of states above the Fermi level. The peak centered around -6.0 eV shows a noticeable broadening and shifts towards higher energies with increased oxidation. This shift suggests a weakening of the initial Pt/O-2p interaction, possibly due to increased competition among oxygen adsorbates for available Pt states.

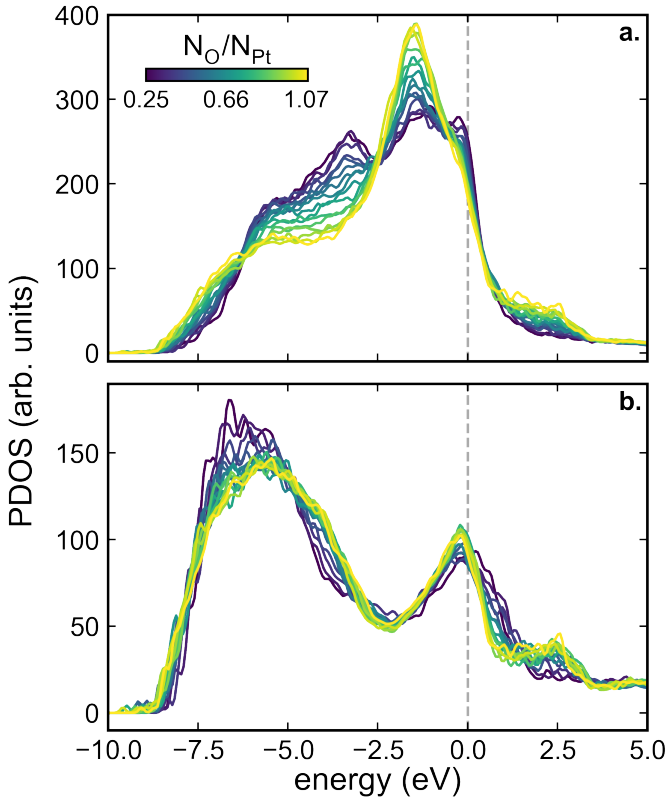

Figure 11: Pt-5d (a) and O-2p (b) PDOS for a range of oxygen ratios as indicated by the color gradient. The Fermi energy, set to 0 eV, is indicated by the vertical dashed line.

Additionally, the appearance of the peak on the Pt-5d PDOS possibly signifies a more molecular-like interaction with O-2p states and the formation of a distinct bonding-antibonding pair with these orbitals. The emergence of O-2p states just above the Fermi level with increasing coverage further supports this interpretation, which would likely represent the

antibonding molecular-like orbital. In Figure 11b, the states close to the Fermi energy, increasing with coverage, are harder to interpret. Considering the average destabilization of the Pt-O bond with increasing oxidation, we suggest that these states are non-bonding or weakly antibonding states. From the perspective of the Pt-5*d* PDOS the slight increase in bandwidth indicates that the interaction should retain metallic character. However, the narrow peak close to the Fermi energy suggests that the ionic nature of these bonds develop as oxygen content increases.

For the O-2*p* PDOS the discussed variations mainly occur at low oxygen ratios (0.25 to 0.6) but vary less at higher ratios. In contrast, the change in Pt-5*d* PDOS is more gradual, suggesting that the Pt structure continuously accommodate to additional oxide species. This suggests that the oxide species are in fixed electronic states for higher oxygen ratios, which can be used to explain the trends observed in Figure 8 which showed an initial important destabilization with oxygen ratio, and a progressive saturation regime observed at higher oxygen ratios.

Interestingly, our Pt-5*d* PDOS trends cannot be linked to both previous theoretical literature and experimental evidence, as both seem to predict inverted trends, i.e. a decrease of intensity close to the Fermi energy with a diffuse increase in intensity for lower states. A DFT study of Verga et al.[30] investigated various oxygen coverages using DFT on perfect nanoparticles, and showed that the density of states clearly shift to lower energies as the oxygen ratio increases, without the presence of a narrow peak below the Fermi energy. This trend is also reported for other metals, such as Pd, Rh, and Cu.[76,77] Similarly, Takagi et al.[28] reported the same behavior experimentally on similarly sized Pt nanoparticles using HAXPES. However, in these studies, nanoparticles are only partially oxidized, e.g. oxygen atoms are only located on the outer shell. This strengthens our conclusion that the features observed in our PDOS are due to a progression towards complete oxidation of the nanoparticle. An additional reason for this discrepancy could be the peculiar geometries given by the ReaxFF forcefield, not entirely addressed even after a MACE-MP-0 geometry optimization.

Additional comparisons will have to be carried out, e.g. by comparing the PDOS of platinum nanoparticles with oxygen only located at the outer shell, or by carrying out the Monte Carlo simulations with a more advanced forcefield such as MACE-MP-0.

Conclusions

We investigated the oxidation behavior of a realistic platinum nanoparticle using a multistep approach combining ReaxFF and MACE-MP-0 forcefields, complemented by DFT calculations. Our Monte Carlo simulations reveal that the nanoparticle becomes highly oxidized at pressures above 10^{-5} atm, with coverage results that are in reasonable agreement with existing literature. To describe the extent of oxidation we performed a spherical shell analysis, effectively plotting the oxygen density around the center of mass. These density profiles show that at high pressures, oxygen atoms are found close to the core. We then attempt to establish a connection between the theoretically predicted complete oxidation and experimental measurements done at different particle size distributions. For our lowest platinum loading sample (10 wt%, 1.7 nm average diameter), we observed predominantly oxidized species with no metallic character from our XRD measurements. Similarly, for the larger sample (20 wt%, 2.4 nm average diameter) XRD did not show a significant crystallite domain. However, our EXAFS analysis showed a low Pt-Pt coordination number from which we conclude that the particles are in a mixed state of metallic and oxidized platinum. These findings suggest that the 1.5 to 2.5 nm size range represents a transitional behavior between larger, partially oxidized nanoparticles and smaller, fully oxidized nanoparticles. We suggest that such Monte Carlo simulations will most likely always predict complete oxidation of the nanoparticle regardless of size due to the lack of kinetic aspects. In reality, however, the oxidation process through to the core is unfavorable for larger nanoparticles due to the high activation energy required for oxygen diffusion into the platinum lattice.

Progressing in our workflow, we carry subsequent molecular dynamics simulations using

the ReaxFF forcefield on the previously obtained geometries from the Monte Carlo simulations. These canonical simulations done at the same temperature of 350K lead to the formation of detached Pt_6O_8 species, previously reported in studies using similar forcefields. We report that the frequency of these detachment events is highly dependent on the oxygen fractional occupancy, with higher occupancies resulting in more numerous detachments. To investigate the plausibility of these species we then performed geometry optimization with the recent MACE-MP-0 forcefield. The forcefield yield structures that do not contain these species, actively trying to systematically reincorporate the detached Pt_6O_8 species into the nanoparticle.

Further exploring the deviations between the two forcefields we conducted binding energy calculations which revealed that ReaxFF predicts stronger binding energies at higher oxygen ratios compared to MACE-MP-0, which we attribute to an artificial stabilization by the Pt_6O_8 species. By comparing the results from both forcefields to our DFT calculations we find that MACE-MP-0 provides binding energies in closer agreement with DFT results, supporting its reliability for describing oxidized platinum nanoparticles. These findings outline the importance of carefully reviewing the applicability of forcefields on a whole range of conditions, in our case, high oxygen ratios are not well described by ReaxFF. A less pronounced plateauing behavior occurring at high oxygen ratios is also observed on the computed binding energies using MACE-MP-0. To investigate the new regime predicted by both forcefields at high oxygen ratios we perform DFT calculations to investigate electronic properties. The projected density of states for Pt-5d orbitals reveals the appearance of intense, narrow peak close to the Fermi energy as oxygen ratio increases, contrasting with previous studies, which suggested a decrease in intensity close to the Fermi energy with a diffuse increase in intensity for lower states. We link this discrepancy to the lack of core oxidation in these previous studies, compared to this work, suggesting that the narrow peak close to the Fermi energy is due to complete oxidation. In contrast, the O-2p PDOS, displays smaller variations, which are localized within the low oxygen ratio range, suggesting that

these species are in fixed electronic states for higher oxygen ratios.

Overall, our findings emphasize the need for caution when using Monte Carlo simulations to study nanoparticle oxidation, as the lack of kinetic aspects can lead to results that are less relevant to catalytic conditions. Additionally, it is important to correctly describe the potential energy surface at a wide range of conditions when using classical forcefields. We report that recent machine learning models such as MACE-MP-0 show promise as a more reliable alternative for studying oxidized platinum nanoparticles, providing geometries and energetics more consistent with DFT calculations. Future work should focus on extending this multistep approach to alloyed systems and investigating the kinetic aspects of oxidation, as the thermodynamic stability of highly oxidized states may not necessarily translate to their practical relevance under catalytic conditions. By combining accurate forcefields, such as MACE-MP-0, with DFT calculations and experimental validation, it may be possible to design more efficient and stable platinum-based catalysts for the oxygen reduction reaction and other important applications. This study serves as a foundation for a more comprehensive understanding of the complex interplay between nanoparticle structure, oxidation state, and catalytic performance, paving the way for the rational design of advanced catalytic materials.

Acknowledgement

The authors acknowledge the use of the IRIDIS High Performance Computing Facility, and associated support services at the University of Southampton, in the completion of this work. We are grateful for access to the ARCHER2 national supercomputer which was obtained via the United Kingdom Car-Parrinello Consortium (UKCP) funded by EPSRC (Grant No. EP/X035956/1). We thank H. Marchbank, A. Phillips, G. Goodlet, and T. Tran for their assistance with experimental measurements. We thank E. Gerouville for proofreading.

Supporting Information Available

The following files are available free of charge.

- `computational_experimental_details.pdf`: Detailed description of the parameters used for both forcefields, Monte Carlo, Molecular Dynamics, and DFT calculations. Description of the experimental methods used for the synthesis and characterization of the nanoparticles. Description of an additional DFT calculation of a lone subsurface oxygen, showing migration towards a 3-fold surface site.

References

(1) Shao, M.; Chang, Q.; Dodelet, J.-P.; Chenitz, R. Recent Advances in Electrocatalysts for Oxygen Reduction Reaction. *Chemical Reviews* **2016**, *116*, 3594–3657.

(2) Sui, S.; Wang, X.; Zhou, X.; Su, Y.; Riffat, S.; Liu, C.-j. A Comprehensive Review of Pt Electrocatalysts for the Oxygen Reduction Reaction: Nanostructure, Activity, Mechanism and Carbon Support in PEM Fuel Cells. *Journal of Materials Chemistry A* **2017**, *5*, 1808–1825.

(3) Stacy, J.; Regmi, Y. N.; Leonard, B.; Fan, M. The Recent Progress and Future of Oxygen Reduction Reaction Catalysis: A Review. *Renewable and Sustainable Energy Reviews* **2017**, *69*, 401–414.

(4) Jung, N.; Chung, D. Y.; Ryu, J.; Yoo, S. J.; Sung, Y.-E. Pt-Based Nanoarchitecture and Catalyst Design for Fuel Cell Applications. *Nano Today* **2014**, *9*, 433–456.

(5) Neyerlin, K. C.; Gu, W.; Jorne, J.; Gasteiger, H. A. Determination of Catalyst Unique Parameters for the Oxygen Reduction Reaction in a PEMFC. *Journal of The Electrochemical Society* **2006**, *153*, A1955.

(6) Jinnouchi, R.; Suzuki, K. K. T.; Morimoto, Y. DFT Calculations on Electro-Oxidations and Dissolutions of Pt and Pt–Au Nanoparticles. *Catalysis Today* **2016**, *262*, 100–109.

(7) Wu, Z.; Yang, G.; Zhang, Q.; Liu, Z.; Peng, F. Deciphering the High Overpotential of the Oxygen Reduction Reaction via Comprehensively Elucidating the Open Circuit Potential. *Energy & Environmental Science* **2024**, *17*, 3338–3346.

(8) Li, Y.; Liu, Z.-F. Solvated Proton and the Origin of the High Onset Overpotential in the Oxygen Reduction Reaction on Pt(111). *Physical Chemistry Chemical Physics* **2020**, *22*, 22226–22235.

(9) Kulkarni, A.; Siahrostami, S.; Patel, A.; Nørskov, J. K. Understanding Catalytic Activity Trends in the Oxygen Reduction Reaction. *Chemical Reviews* **2018**, *118*, 2302–2312.

(10) Montemore, M. M.; van Spronsen, M. A.; Madix, R. J.; Friend, C. M. O2 Activation by Metal Surfaces: Implications for Bonding and Reactivity on Heterogeneous Catalysts. *Chemical Reviews* **2018**, *118*, 2816–2862.

(11) Gland, J. L. Molecular and Atomic Adsorption of Oxygen on the Pt(111) and Pt(S)-12(111) × (111) Surfaces. *Surface Science* **1980**, *93*, 487–514.

(12) Gland, J. L.; Sexton, B. A.; Fisher, G. B. Oxygen Interactions with the Pt(111) Surface. *Surface Science* **1980**, *95*, 587–602.

(13) Derry, G. N.; Ross, P. N. High Coverage States of Oxygen Adsorbed on Pt(100) and Pt(111) Surfaces. *Surface Science* **1984**, *140*, 165–180.

(14) Campbell, C. T.; Ertl, G.; Kuipers, H.; Segner, J. A Molecular Beam Study of the Adsorption and Desorption of Oxygen from a Pt(111) Surface. *Surface Science* **1981**, *107*, 220–236.

(15) Peuckert, M.; Bonzel, H. P. Characterization of Oxidized Platinum Surfaces by X-ray Photoelectron Spectroscopy. *Surface Science* **1984**, *145*, 239–259.

(16) Parker, D. H.; Bartram, M. E.; Koel, B. E. Study of High Coverages of Atomic Oxygen on the Pt(111) Surface. *Surface Science* **1989**, *217*, 489–510.

(17) Devarajan, S. P.; Hinojosa, J. A.; Weaver, J. F. STM Study of High-Coverage Structures of Atomic Oxygen on Pt(111): P(2×1) and Pt Oxide Chain Structures. *Surface Science* **2008**, *602*, 3116–3124.

(18) Fantauzzi, D.; Krick Calderón, S.; Mueller, J. E.; Grabau, M.; Papp, C.; Steinrück, H.-P.; Senftle, T. P.; van Duin, A. C. T.; Jacob, T. Growth of Stable Surface Oxides on Pt(111) at Near-Ambient Pressures. *Angewandte Chemie International Edition* **2017**, *56*, 2594–2598.

(19) Zhu, Z.; Tao, F. F.; Zheng, F.; Chang, R.; Li, Y.; Heinke, L.; Liu, Z.; Salmeron, M.; Somorjai, G. A. Formation of Nanometer-Sized Surface Platinum Oxide Clusters on a Stepped Pt(557) Single Crystal Surface Induced by Oxygen: A High-Pressure STM and Ambient-Pressure XPS Study. *Nano Letters* **2012**, *12*, 1491–1497.

(20) Ellinger, C.; Stierle, A.; Robinson, I. K.; Nefedov, A.; Dosch, H. Atmospheric Pressure Oxidation of Pt(111). *Journal of Physics: Condensed Matter* **2008**, *20*, 184013.

(21) Chen, J.; Lim, B.; Lee, E. P.; Xia, Y. Shape-Controlled Synthesis of Platinum Nanocrystals for Catalytic and Electrocatalytic Applications. *Nano Today* **2009**, *4*, 81–95.

(22) Seriani, N.; Mittendorfer, F. Platinum-Group and Noble Metals under Oxidizing Conditions. *Journal of Physics: Condensed Matter* **2008**, *20*, 184023.

(23) Wang, H.; Wang, Y.; Zhu, Z.; Sapi, A.; An, K.; Kennedy, G.; Michalak, W. D.; Somorjai, G. A. Influence of Size-Induced Oxidation State of Platinum Nanoparticles on Selectivity and Activity in Catalytic Methanol Oxidation in the Gas Phase. *Nano Letters* **2013**, *13*, 2976–2979.

(24) Şen, F.; Gökağaç, G. Different Sized Platinum Nanoparticles Supported on Carbon: An XPS Study on These Methanol Oxidation Catalysts. *The Journal of Physical Chemistry C* **2007**, *111*, 5715–5720.

(25) Saveleva, V. A.; Papaefthimiou, V.; Daletou, M. K.; Doh, W. H.; Ulhaq-Bouillet, C.; Diebold, M.; Zafeiratos, S.; Savinova, E. R. Operando Near Ambient Pressure XPS (NAP-XPS) Study of the Pt Electrochemical Oxidation in H2O and H2O/O2 Ambients. *The Journal of Physical Chemistry C* **2016**, *120*, 15930–15940.

(26) Imai, H.; Izumi, K.; Matsumoto, M.; Kubo, Y.; Kato, K.; Imai, Y. In Situ and Real-Time Monitoring of Oxide Growth in a Few Monolayers at Surfaces of Platinum Nanoparticles in Aqueous Media. *Journal of the American Chemical Society* **2009**, *131*, 6293–6300.

(27) Banerjee, R.; Chen, D. A.; Karakalos, S.; Piedboeuf, M.-L. C.; Job, N.; Regalbuto, J. R. Ambient Oxidation of Ultrasmall Platinum Nanoparticles on Microporous Carbon Catalyst Supports. *ACS Applied Nano Materials* **2018**, *1*, 5876–5884.

(28) Takagi, Y.; Wang, H.; Uemura, Y.; Nakamura, T.; Yu, L.; Sekizawa, O.; Uruga, T.; Tada, M.; Samjeské, G.; Iwasawa, Y. et al. In Situ Study of Oxidation States of Platinum Nanoparticles on a Polymer Electrolyte Fuel Cell Electrode by near Ambient Pressure Hard X-ray Photoelectron Spectroscopy. *Physical Chemistry Chemical Physics* **2017**, *19*, 6013–6021.

(29) Yoshida, H.; Omote, H.; Takeda, S. Oxidation and Reduction Processes of Platinum Nanoparticles Observed at the Atomic Scale by Environmental Transmission Electron Microscopy. *Nanoscale* **2014**, *6*, 13113–13118.

(30) Verga, L. G.; Aarons, J.; Sarwar, M.; Thompsett, D.; Russell, A. E.; Skylaris, C.-K. DFT Calculation of Oxygen Adsorption on Platinum Nanoparticles: Coverage and Size Effects. *Faraday Discussions* **2018**, *208*, 497–522.

(31) Kirchhoff, B.; Braunwarth, L.; Jung, C.; Jónsson, H.; Fantauzzi, D.; Jacob, T. Simulations of the Oxidation and Degradation of Platinum Electrocatalysts. *Small* **2020**, *16*, 1905159.

(32) Kirchhoff, B.; Jung, C.; Jónsson, H.; Fantauzzi, D.; Jacob, T. Simulations of the Electrochemical Oxidation of Pt Nanoparticles of Various Shapes. *The Journal of Physical Chemistry C* **2022**, *126*, 6773–6781.

(33) Slapikas, R.; Dabo, I.; Sinnott, S. B. Surface Reconstruction of Oxidized Platinum Nanoparticles Using Classical Molecular Dynamics Simulations. *Computational Materials Science* **2022**, *209*, 111364.

(34) Lim, D.-H.; Wilcox, J. DFT-Based Study on Oxygen Adsorption on Defective Graphene-Supported Pt Nanoparticles. *The Journal of Physical Chemistry C* **2011**, *115*, 22742–22747.

(35) Aarons, J.; Jones, L.; Varambhia, A.; MacArthur, K. E.; Ozkaya, D.; Sarwar, M.; Skylaris, C.-K.; Nellist, P. D. Predicting the Oxygen-Binding Properties of Platinum Nanoparticle Ensembles by Combining High-Precision Electron Microscopy and Density Functional Theory. *Nano Letters* **2017**, *17*, 4003–4012.

(36) Ellaby, T.; Aarons, J.; Varambhia, A.; Jones, L.; Nellist, P.; Ozkaya, D.; Sarwar, M.; Thompsett, D.; Skylaris, C.-K. Ideal versus Real: Simulated Annealing of Experimentally Derived and Geometric Platinum Nanoparticles. *Journal of Physics: Condensed Matter* **2018**, *30*, 155301.

(37) van Duin, A. C. T.; Dasgupta, S.; Lorant, F.; Goddard, W. A. ReaxFF: A Reactive Force Field for Hydrocarbons. *The Journal of Physical Chemistry A* **2001**, *105*, 9396–9409.

(38) Batatia, I.; Benner, P.; Chiang, Y.; Elena, A. M.; Kovács, D. P.; Riebesell, J.; Advincula, X. R.; Asta, M.; Baldwin, W. J.; Bernstein, N. et al. A Foundation Model for Atomistic Materials Chemistry. 2023.

(39) Aktulga, H. M.; Fogarty, J. C.; Pandit, S. A.; Grama, A. Y. Parallel Reactive Molecular Dynamics: Numerical Methods and Algorithmic Techniques. *Parallel Computing* **2012**, *38*, 245–259.

(40) Thompson, A. P.; Aktulga, H. M.; Berger, R.; Bolintineanu, D. S.; Brown, W. M.; Crozier, P. S.; in 't Veld, P. J.; Kohlmeyer, A.; Moore, S. G.; Nguyen, T. D. et al. LAMMPS - a Flexible Simulation Tool for Particle-Based Materials Modeling at the Atomic, Meso, and Continuum Scales. *Computer Physics Communications* **2022**, *271*, 108171.

(41) Gai, L.; Shin, Y. K.; Raju, M.; Van Duin, A. C. T.; Raman, S. Atomistic Adsorption of Oxygen and Hydrogen on Platinum Catalysts by Hybrid Grand Canonical Monte Carlo/Reactive Molecular Dynamics. *The Journal of Physical Chemistry C* **2016**, *120*, 9780–9793.

(42) Fantauzzi, D.; Bandlow, J.; Sabo, L.; Mueller, J. E.; van Duin, A. C. T.; Jacob, T. Development of a ReaxFF Potential for Pt–O Systems Describing the Energetics and Dynamics of Pt-oxide Formation. *Physical Chemistry Chemical Physics* **2014**, *16*, 23118–23133.

(43) Allison, T. C. NIST-JANAF Thermochemical Tables - SRD 13. 2013.

(44) Batatia, I.; Kovács, D. P.; Simm, G. N. C.; Ortner, C.; Csányi, G. MACE: Higher Order Equivariant Message Passing Neural Networks for Fast and Accurate Force Fields. 2023.

(45) Riebesell, J.; Goodall, R. E. A.; Benner, P.; Chiang, Y.; Deng, B.; Lee, A. A.; Jain, A.; Persson, K. A. Matbench Discovery – A Framework to Evaluate Machine Learning Crystal Stability Predictions. 2024.

(46) Prentice, J. C. A.; Aarons, J.; Womack, J. C.; Allen, A. E. A.; Andrinopoulos, L.; Anton, L.; Bell, R. A.; Bhandari, A.; Bramley, G. A.; Charlton, R. J. et al. The

ONETEP Linear-Scaling Density Functional Theory Program. *The Journal of Chemical Physics* **2020**, *152*, 174111.

(47) Ruiz-Serrano, Á.; Skylaris, C.-K. A Variational Method for Density Functional Theory Calculations on Metallic Systems with Thousands of Atoms. *The Journal of Chemical Physics* **2013**, *139*, 054107.

(48) C. Jennings, P.; A. Aleksandrov, H.; M. Neyman, K.; L. Johnston, R. DFT Studies of Oxygen Dissociation on the 116-Atom Platinum Truncated Octahedron Particle. *Physical Chemistry Chemical Physics* **2014**, *16*, 26539–26545.

(49) G. Yohannes, A.; Fink, K.; Kondov, I. Pt Nanoparticles under Oxidizing Conditions – Implications of Particle Size, Adsorption Sites and Oxygen Coverage on Stability. *Nanoscale Advances* **2022**, *4*, 4554–4569.

(50) Légaré, P. Interaction of Oxygen with the Pt(111) Surface in Wide Conditions Range. A DFT-based Thermodynamical Simulation. *Surface Science* **2005**, *580*, 137–144.

(51) Gu, Z.; Balbuena, P. B. Absorption of Atomic Oxygen into Subsurfaces of Pt(100) and Pt(111): Density Functional Theory Study. *The Journal of Physical Chemistry C* **2007**, *111*, 9877–9883.

(52) Hawkins, J. M.; Weaver, J. F.; Asthagiri, A. Density Functional Theory Study of the Initial Oxidation of the Pt(111) Surface. *Physical Review B* **2009**, *79*, 125434.

(53) Getman, R. B.; Schneider, W. F.; Smeltz, A. D.; Delgass, W. N.; Ribeiro, F. H. Oxygen-Coverage Effects on Molecular Dissociations at a Pt Metal Surface. *Physical Review Letters* **2009**, *102*, 076101.

(54) Calle-Vallejo, F. The ABC of Generalized Coordination Numbers and Their Use as a Descriptor in Electrocatalysis. *Advanced Science* **2023**, *10*, 2207644.

(55) Tada, M.; Murata, S.; Asakoka, T.; Hiroshima, K.; Okumura, K.; Tanida, H.; Uruga, T.; Nakanishi, H.; Matsumoto, S.-i.; Inada, Y. et al. In Situ Time-Resolved Dynamic Surface Events on the Pt/C Cathode in a Fuel Cell under Operando Conditions. *Angewandte Chemie International Edition* **2007**, *46*, 4310–4315.

(56) Nomiyama, R. K.; Piotrowski, M. J.; Da Silva, J. L. F. Bulk Structures of PtO and PtO 2 from Density Functional Calculations. *Physical Review B* **2011**, *84*, 100101.

(57) Seriani, N.; Pompe, W.; Ciacchi, L. C. Catalytic Oxidation Activity of Pt3O4 Surfaces and Thin Films. *The Journal of Physical Chemistry B* **2006**, *110*, 14860–14869.

(58) Bugaris, D. E.; Smith, M. D.; zur Loye, H.-C. Hydroflux Crystal Growth of Platinum Group Metal Hydroxides: Sr6NaPd2(OH)17, Li2Pt(OH)6, Na2Pt(OH)6, Sr2Pt(OH)8, and Ba2Pt(OH)8. *Inorganic Chemistry* **2013**, *52*, 3836–3844.

(59) Zurhelle, A. F.; Stehling, W.; Waser, R.; De Souza, R. A.; Menzel, S. Oxygen Diffusion in Platinum Electrodes: A Molecular Dynamics Study of the Role of Extended Defects. *Advanced Materials Interfaces* **2022**, *9*, 2101257.

(60) Takao, S.; Sekizawa, O.; Samjeské, G.; Kaneko, T.; Higashi, K.; Yoshida, Y.; Zhao, X.; Sakata, T.; Yamamoto, T.; Gunji, T. et al. Observation of Degradation of Pt and Carbon Support in Polymer Electrolyte Fuel Cell Using Combined Nano-X-ray Absorption Fine Structure and Transmission Electron Microscopy Techniques. *ACS Applied Materials & Interfaces* **2018**, *10*, 27734–27744.

(61) Fuchs, T.; Drnec, J.; Calle-Vallejo, F.; Stubb, N.; Sandbeck, D. J. S.; Ruge, M.; Cherevko, S.; Harrington, D. A.; Magnussen, O. M. Structure Dependency of the Atomic-Scale Mechanisms of Platinum Electro-Oxidation and Dissolution. *Nature Catalysis* **2020**, *3*, 754–761.

(62) Nørskov, J. K.; Rossmeisl, J.; Logadottir, A.; Lindqvist, L.; Kitchin, J. R.; Bligaard, T.;

Jónsson, H. Origin of the Overpotential for Oxygen Reduction at a Fuel-Cell Cathode. *The Journal of Physical Chemistry B* **2004**, *108*, 17886–17892.

(63) Sargeant, E.; Illas, F.; Rodríguez, P.; Calle-Vallejo, F. Importance of the Gas-Phase Error Correction for O2 When Using DFT to Model the Oxygen Reduction and Evolution Reactions. *Journal of Electroanalytical Chemistry* **2021**, *896*, 115178.

(64) Alfonso, D.; Tafen, D.; Kauffmann, D. First-Principles Modeling in Heterogeneous Electrocatalysis. *Catalysts* **2018**, *8*, 424.

(65) Farkas, A.; Fantauzzi, D.; Mueller, J. E.; Zhu, T.; Papp, C.; Steinrück, H.-P.; Jacob, T. On the Platinum-Oxide Formation under Gas-Phase and Electrochemical Conditions. *Journal of Electron Spectroscopy and Related Phenomena* **2017**, *221*, 44–57.

(66) Huang, J.; Zhang, J.; Eikerling, M. Unifying Theoretical Framework for Deciphering the Oxygen Reduction Reaction on Platinum. *Physical Chemistry Chemical Physics* **2018**, *20*, 11776–11786.

(67) Wakisaka, M.; Suzuki, H.; Mitsui, S.; Uchida, H.; Watanabe, M. Identification and Quantification of Oxygen Species Adsorbed on Pt(111) Single-Crystal and Polycrystalline Pt Electrodes by Photoelectron Spectroscopy. *Langmuir* **2009**, *25*, 1897–1900.

(68) Casalongue, H. S.; Kaya, S.; Viswanathan, V.; Miller, D. J.; Friebel, D.; Hansen, H. A.; Nørskov, J. K.; Nilsson, A.; Ogasawara, H. Direct Observation of the Oxygenated Species during Oxygen Reduction on a Platinum Fuel Cell Cathode. *Nature Communications* **2013**, *4*, 2817.

(69) Chen, W.; Huang, J.; Wei, J.; Zhou, D.; Cai, J.; He, Z.-D.; Chen, Y.-X. Origins of High Onset Overpotential of Oxygen Reduction Reaction at Pt-based Electrocatalysts: A Mini Review. *Electrochemistry Communications* **2018**, *96*, 71–76.

(70) You, H.; Zurawski, D. J.; Nagy, Z.; Yonco, R. M. *In-Situ* x-Ray Reflectivity Study of Incipient Oxidation of Pt(111) Surface in Electrolyte Solutions. *The Journal of Chemical Physics* **1994**, *100*, 4699–4702.

(71) You, H.; Nagy, Z. Oxidation-Reduction-Induced Roughening of Platinum (1 1 1) Surface. *Physica B: Condensed Matter* **1994**, *198*, 187–194.

(72) Teliska, M.; O'Grady, W. E.; Ramaker, D. E. Determination of O and OH Adsorption Sites and Coverage in Situ on Pt Electrodes from Pt L $_{23}$ X-ray Absorption Spectroscopy. *The Journal of Physical Chemistry B* **2005**, *109*, 8076–8084.

(73) Zhu, T.; Hensen, E. J. M.; Van Santen, R. A.; Tian, N.; Sun, S.-G.; Kaghazchi, P.; Jacob, T. Roughening of Pt Nanoparticles Induced by Surface-Oxide Formation. *Physical Chemistry Chemical Physics* **2013**, *15*, 2268.

(74) Hörmann, N. G.; Andreussi, O.; Marzari, N. Grand Canonical Simulations of Electrochemical Interfaces in Implicit Solvation Models. *The Journal of Chemical Physics* **2019**, *150*, 041730.

(75) Guidelli, R.; Schmickler, W. In *Modern Aspects of Electrochemistry*; Conway, B. E., Vayenas, C. G., White, R. E., Gamboa-Adelco, M. E., Eds.; Springer US: Boston, MA, 2005; Vol. 38; pp 303–371.

(76) İnoğlu, N.; Kitchin, J. R. Simple Model Explaining and Predicting Coverage-Dependent Atomic Adsorption Energies on Transition Metal Surfaces. *Physical Review B* **2010**, *82*, 045414.

(77) Kitchin, J. R. Correlations in Coverage-Dependent Atomic Adsorption Energies on Pd(111). *Physical Review B* **2009**, *79*, 205412.